This is a repository copy of *Novel method to achieve temperature-stable microwave dielectric ceramics: a case in the fergusonite-structured NdNbO4 system*.

White Rose Research Online URL for this paper:
https://eprints.whiterose.ac.uk/198314/

Version: Accepted Version

Novel Method to Achieve Temperature Stable Microwave Dielectric Ceramics: A Case in Fergusonite Structured NdNbO$_4$ System

Di Zhou,[*a] Ling Zhang,[a] Di-Ming Xu,[a] Feng Qiao,[a] Xiaogang Yao,[b] Huixing Lin,[b]

Wenfeng Liu,[c] Li-Xia Pang,[d] Fayaz Hussain,[e] Moustafa Adel Darwish,[f] Tao Zhou,[g]

Yawei Chen,[h] Qixin Liang[h] & Meirong Zhang[h] & Ian M. Reaney[*i]

[a]Electronic Materials Research Laboratory, Key Laboratory of the Ministry of Education &

International Center for Dielectric Research, School of Electronic Science and Engineering,

Xi'an Jiaotong University, Xi'an 710049, Shaanxi, China

[b]Key Laboratory of Inorganic Functional Material and Device, Shanghai Institute of Ceramics

Chinese Academy of Sciences, Shanghai 200050, China

[c]State Key Laboratory of Electrical Insulation and Power Equipment, Xi'an Jiaotong

University, Xi'an 710049, Shaanxi, China

[d]Micro-optoelectronic Systems Laboratories, Xi'an Technological University, Xi'an 710032,

Shaanxi, China

[e]Department of Materials Engineering, NED University of Engineering & Technology,

Karachi, 75270, Pakistan

[f]Physics Department, Faculty of Science, Tanta University, Al-Geish st., Tanta 31527, Egypt

[g]School of Electronic and Information Engineering, Hangzhou Dianzi University, Hangzhou,

310018, China

[h]Shenzhen Microgate Technology Co., Ltd., Shen Zhen, 518118, Guang Dong

Province, China

[i]Functional Materials and Devices Group, Department of Materials Science and Engineering,

University of Sheffield, S1 3JD, UK

[*]Corresponding author E-mail address: zhoudi1220@gmail.com (Di Zhou) & i.m.reaney@sheffield.ac.uk (Ian M. Reaney)

ABSTRACT

Microwave dielectric ceramics with permittivity (ε_r) ~ 20 play an important role in massive multiple-input multiple-output (MIMO) technology in 5G. Although fergusonite-structured materials with low dielectric loss are good candidates for 5G application, tuning the temperature coefficient of resonant frequency (TCF) remains a problem. In the present work, smaller V^{5+} ions (r_V = 0.355 Å, with coordination number (C.N.) = 4) were substituted for Nb^{5+} (r_{Nb} = 0.48 Å with C.N. = 4) in the $Nd(Nb_{1-x}V_x)O_4$ ceramics which, according to *in-situ* X-ray diffraction data, lowered the fergusonite to scheelite phase transition (T_{F-S}) to 400 °C for x = 0.2. The thermal expansion coefficient (α_L) of the high temperature scheelite phase was +11 ppm/°C, whereas for the low temperature fergusonite phase + 14 < α_L < + 15 ppm/°C. The abrupt change in α_L, the associated negative temperature coefficient of permittivity (τ_ε) and the minimum value of ε_r at T_{F-S} resulted in a near-zero TCF ~ (+ 7.8 ppm/°C) for the $Nd(Nb_{0.8}V_{0.2})O_4$ (ε_r ~ 18.6 and Qf ~ 70,100 GHz). A method to design near-zero TCF compositions based on modulation of τ_ε and α_L at T_{F-S} is thus demonstrated that may also be extended to other fergusonite systems.

Keywords: Microwave dielectric ceramics; Fergusonite; Scheelite; Dielectric Resonator; Temperature coefficient of resonant frequency

1. Introduction

Dielectric ceramics play a key role in modern microwave devices as dielectric resonators and filters, antenna substrates, class I multilayer capacitors and low temperature co-fired ceramics (LTCC).[1-5] With the development of 5th generation technology (5G), demand of dielectric filters with ultra-high quality factors (Q=1/dielectric loss) is increasing for massive MIMO (multiple-input multiple-output) technology, which is widely used in the current generation of 5G base stations (sub-6 GHz).[6-9] The resonant frequency (f) is well-known to be proportional to the inverse square route of dielectric constant / permittivity (ε_r) ($f \propto \frac{1}{\sqrt{\varepsilon_r}}$) and ceramics with $\varepsilon_r \sim 20$ (commercially referred to as K20) are suitable for dielectric filters working at sub-6 GHz with dimensions of the order of a few centimeters.

Now, the market for K20 ceramics is mainly met by $MgTiO_3$-(Ca, Sr, Ln)TiO_3 or Mg_2TiO_4-(Ca, Sr, Ln)TiO_3 (Ln = Lanthanides) due to the low-cost, acceptable Qf (> 60,000 GHz) and low bulk density (3.6 g/cm^3).[10-16] The main phase of this system is ilmenite-structured $MgTiO_3$ which has a high Qf but negative temperature coefficient of frequency (TCF) which is compensated by $CaTiO_3$ which has a large positive TCF. However, microwave dielectric properties of this system are unstable over the whole of the anticipated working temperature (– 55 °C to + 125 °C). Compared with $MgTiO_3$-$CaTiO_3$ system, the Ruddlesden-Popper structured CaLnAlO$_4$-Ca_2TiO_4 (Ln = lanthanide) system usually has a higher Qf (90,000 GHz) and a wider range of temperature stability[17-22] but its bulk density is 4.9 g/cm^3, adding unnecessary weight to 5G base stations. Moreover, Li_2TiO_3 solid solutions have also caught massive attention due to their high Qf (>90,000 GHz) and relative low sintering temperature < 1150 °C[23-26] but the weak solubility of Li_2CO_3 in water adds complexity and cost to

ceramic fabrication. Microwave dielectric properties of the above systems are summarized in Table 1.

In addition to the above three ceramic systems, fergusonite-structured LnNbO$_4$ (Ln = lanthanide) is also a potential K20 microwave dielectric with high Qf (>30,000 GHz). LnNbO$_4$ series materials undergo ferroelastic phase transition from monoclinic fergusonite to tetragonal scheelite structure whose temperature (T$_{F-S}$) varies with the Ln ion radius from ~ 480°C of LaNbO$_4$ to 860°C of SmNbO$_4$.[3,27-33] In the previous work,[33] we have demonstrated anomalous dielectric behavior in La(Nb$_{0.9}$V$_{0.1}$)O$_4$ such that a minimum (not a usual maximum value at phase transition temperature) of ε$_r$ is observed at T$_{F-S}$ (~350 °C). This phenomenon was explained by a combination of the Shannon's additive rule and Clausius–Mosotti relation based on the assumption of linear increases in ionic polarizabilities. Here, an unique ε$_r$ minimum is explored to design a temperature-independent K20 microwave dielectric ceramic with high Qf in the solid solution, Nd(Nb$_{1-x}$V$_x$)O$_4$.

2. Materials and methods

a) Sample preparation.

Traditional solid state reaction method was employed to prepare the Nd(Nb$_{1-x}$V$_x$)O$_4$ ($0 \leq x \leq 0.2$) (x = 0, 0.1 and 0.2) ceramics, using Nd$_2$O$_3$ (> 99.9%), V$_2$O$_5$, (> 99.2%) and Nb$_2$O$_5$ (> 99.5%) as initial materials, with a calcination temperature ~ 1150 °C and sintering temperatures between 1250 °C to 1350 °C in air.

b) Characterization and Electrical measurements.

Room temperature powder X-ray diffraction (PXRD) was performed using with CuKα radiation (Bruker D2 Phaser) in the range of 10-75 ° with a step size of 0.02 °. PXRD patterns at high temperatures were collected using a Siemens D5000 diffractometer upon Pt foil holder from 25 to 700 °C. FULLPROF program was

selected to perform the refinements. Thermally etched surfaces were observed by using scanning electron microscopy (SEM, FEI, Inspect F). Thermal expansion data were monitored in temperature range from 25 to 750 °C. Dielectric properties were obtained over gold coated ceramics from 25 to 700 °C with a heating/cooling rate of 1 °C/min using a LCR meter (Agilent E4980A) in a temperature chamber at frequencies 100 kHz ~ 1 MHz. Room temperature infrared spectra were collected using a Bruker IFS 66v FT-IR spectrometer at the National Synchrotron Radiation Lab (NSRL), China (Infrared beamline station, U4). Dielectric properties at microwave frequencies (about 7 GHz) were measured using the $TE_{01\delta}$ method[34] with a network vector analyzer equipped with a home-made heating system. Temperature coefficients of resonant frequency TCF/τ_f were calculated according to the following equation:

$$TCF(\tau_f) = \frac{f_{85} - f_{25}}{f_{25} \times (85 - 25)} \times 10^6 \qquad (1)$$

where f_{85} and f_{25} are the $TE_{01\delta}$ resonant frequencies at 85 °C and 25 °C, respectively.

3. Results and Discussions

As shown in Fig. 1, all the $Nd(Nb_{1-x}V_x)O_4$ ceramics crystallize in the fergusonite structure with no secondary phase, indicating that V feasibly substitutes Nb in the system. The crystal structure and PXRD data refinement profiles of $Nd(Nb_{0.9}V_{0.1})O_4$ and $Nd(Nb_{0.8}V_{0.2})O_4$ ceramics are shown in Fig. 1(e) and (f), giving the refined unit cell parameters of the $Nd(Nb_{0.9}V_{0.1})O_4$ ceramic at 25 °C of a = 5.4367(5) Å, b = 11.3356(6) Å, c = 5.1590 (7) Å, β = 93.699(3)°, with the space group $I12/c1$ (No. 15) and a = 5.3982(9) Å, b = 11.3828(7) Å, c = 5.1751(9) Å, β = 92.865(1)°, with space group $I12/c1$ (No. 15) of $Nd(Nb_{0.8}V_{0.2})O_4$. All the details of refinements are presented in Table 2 and Table 3. Form the XRD patterns, as x increases, the $(1\bar{2}1)$ and the (031)

peaks gradually converge, suggesting that the β angle in the unit cell continuously decreases to ~ 90 degrees. Fig. 1(b) and (c) present the *in-situ* PXRD patterns from 25 to 700 $^\circ$C and 25 to 500 $^\circ$C for $Nd(Nb_{0.9}V_{0.1})O_4$ and $Nd(Nb_{0.8}V_{0.2})O_4$, respectively. The characteristic peaks $(011)/(110)$, $(1\bar{2}1)/(031)$, $(002)/(200)$ move closer to each other as temperature increases and eventually merge into respective single-peaks at 600 $^\circ$C and 400 $^\circ$C of $Nd(Nb_{0.9}V_{0.1})O_4$ and $Nd(Nb_{0.8}V_{0.2})O_4$, respectively, again demonstrating that the crystal structure changes continuously from the monoclinic fergusonite structure to the tetragonal scheelite one. Compared with Nb^{5+} (0.48 Å in tetrahedron), V^{5+} has a smaller ionic radius (0.355 Å with CN = 4)[35] and the substitution over Nb in the fergusonite structure diminishes the distortion of the tetrahedra, as shown in the schematic of Fig. 1(d). Nb^{5+} ions prefer 6 coordinated environment in most circumstances, for instance, $BiNbO_4$, $Ba(Zn_{1/3}Nb_{2/3})O_3$ etc.[36,37] However, in the monoclinic fergusonite structure, Nb^{5+} ions are effectively 4-coordinated due to two of the Nb-O bonds are significantly longer than the other four (2.47 Å $\gg$ 1.92 Å $>$ 1.84 Å). In most compounds, V^{5+} ions are 4 coordinated[38] and the subsequent substitution over Nb^{5+} results in a reduction of the degree of distortion at the BO_4 tetrahedra. Correspondingly, a decrease of the ferroelastic phase transition temperature from 720 $^\circ$C ($NdNbO_4$) to 400 $^\circ$C ($Nd(Nb_{0.8}V_{0.2})O_4$) was observed.

The unit cell parameters of $Nd(Nb_{0.9}V_{0.1})O_4$ and $Nd(Nb_{0.8}V_{0.2})O_4$ as a function of temperature are plotted in Fig. 2(a), derived from the high temperatures PXRD refinement results. As temperature increases, the unit cell parameter a decreases while c increases accompanied by a decrease in β. At the temperature point T_{F-S}, a and c become equal and the β angle resolves to 90°, indicating the occurrence of the phase transition to the tetragonal scheelite structure. b continuously increases in the whole

temperature range and is much larger than a and c. The cell volumes of $Nd(Nb_{0.9}V_{0.1})O_4$ and $Nd(Nb_{0.8}V_{0.2})O_4$ present similar change trends to those of b. This may be the reason of the abrupt change in thermal expansion coefficient at T_{F-S}, see Fig. 2b, from +14 ~ +15 ppm/°C to +11 ppm/°C of the fergusonite and the scheelite phases, respectively. This anomaly in thermal expansion was first observed in $La(Nb_{0.9}V_{0.1})O_4$ at the T_{F-S} transition point and also in $BiVO_4$ at the monoclinic to tetragonal scheelite structure transition temperature point.[33,38]

Further HRTEM images were captured to illustrate the relationship among V substitution, microstructure and dielectric properties, as seen from Fig. 3. Clear domain regions and lattice fringes could be observed in both $Nd(Nb_{0.9}V_{0.1})O_4$ and $Nd(Nb_{0.8}V_{0.2})O_4$ ceramics. Meanwhile, the differences between the two sets of HRTEM images are apparent. With a larger amount of V substitution, the size of the domains reduces from 28(2) nm, $x = 0.1$, to 9.6(6) nm, $x = 0.2$, along with the (2 0 0) plane average interplanar spacing reduction from 2.62(3) Å, $x = 0.1$, to 2.53(3) Å, $x = 0.2$. The result is not surprising because of the ionic radii difference. This may also be the reason for the present of the anomaly in the temperature-dependent dielectric permittivity spectra. Moreover, the domain alternation could be indicated as ~ 94 ° rotation, equivalent to the β angle.

SEM images of the $Nd(Nb_{1-x}V_x)O_4$ ($0 \leq x \leq 0.2$) solid solution ceramics are shown in Fig. 4. The microstructures present homogeneous and dense (> 98.5% relative) in all the ceramics sintered at optimal temperatures. However, the substitution of Nb by V did not lower the sintering temperature remarkably as expected but could decrease the grain size from 4 ~ 8 μm to 1 ~ 3 μm.

The dielectric permittivity ε_r and the dielectric loss of the $Nd(Nb_{1-x}V_x)O_4$ ($x = 0.1$ and 0.2) ceramics as a function of temperature at 100 kHz, 250 kHz, 1 MHz and 7.2

GHz are plotted in Fig. 5. ε_r of $Nd(Nb_{0.9}V_{0.1})O_4$ and $Nd(Nb_{0.8}V_{0.2})O_4$ ceramics reach their minimum value at T_{F-S}, concomitant with the change trend of the thermal expansion coefficient and also seen in the $La(Nb_{0.9}V_{0.1})O_4$].[33] The correlation of the change in thermal expansion coefficient and ε_r relates to the change in cell volume and its influence on ionic polarizability at T_{F-S}.[33] Notably, the dielectric anomaly is frequency-dependent in $Nd(Nb_{0.9}V_{0.1})O_4$ but not in $Nd(Nb_{0.8}V_{0.2})O_4$. Moreover, there is a secondary broad anomaly in $Nd(Nb_{0.9}V_{0.1})O_4$ in the range of 25 ~ 200 ^oC but is absent in $Nd(Nb_{0.8}V_{0.2})O_4$, both of which require further investigation. Limited by the equipment, microwave dielectric properties at 7.2 GHz were obtained from room temperature to 120 ^oC. The ε_r at 7.2 GHz data is smaller than that measured at lower frequencies but shows a similar trend, supporting the calculated TCF value.

The microwave dielectric properties (ε_r, Qf and TCF) of the $Nd(Nb_{1-x}V_x)O_4$ ($0 \leq x \leq 0.2$) ceramics as a function of x are presented in Fig. 6. ε_r decreased linearly from 19.6 of $NdNbO_4$ to 18.6 of $Nd(Nb_{0.8}V_{0.2})O_4$, which could be attributed to the smaller ionic polarizability of V^{5+} than that of Nb^{5+} (2.92 $Å^3$ < 3.97 $Å^3$).[33,38-41] The Qf value increases from ~ 33,000 GHz to ~ 70,100 GHz as x increases from 0 to 0.2, along with the TCF shifts from − 39 ppm/^oC to + 7.8 ppm/^oC. The latter may be understood by ε_r-temperature dependence and thermal expansion associated with T_{F-S} transition. The relation function between TCF and temperature-dependence of permittivity could be written as

$$TCF = -(\alpha_L + 1/2\tau_\varepsilon) \tag{2}$$

in which τ_ε is the temperature coefficient of ε_r and α_L is the linear thermal expansion. As x increases to 0.2, the decrease in ε_r at 400 °C leads to a negative τ_ε value, which is opposite to the positive thermal expansion coefficient and correspondingly resulting in near zero TCF. Phase transition temperatures obtained from the *in-situ* XRD were

also plotted in Fig. 6(b). It is clearly that at room temperature all the $Nd(Nb_{1-x}V_x)O_4$ ceramics belong to single fergusonite structure and the modifications of TCF can be attributed totally to the complex influence of negative τ_ε and positive α_L values. To avoid other extrinsic influence, such as space charge polarizations and dipole polarizations, we further studied intrinsic dielectric properties of the $Nd(Nb_{1-x}V_x)O_4$ (x = 0.1 and 0.2) ceramics, far-infrared reflectivity spectra were fitted to calculate the complex permittivity (ε_r) as shown in Fig. 7. Good agreements of measured and fitted infrared spectra were obtained and the extrapolated ε_r to the microwave region agrees well with the measured values by $TE_{01\delta}$ method, which further confirms that only the lattice vibrations at infrared region of the $Nd(Nb_{1-x}V_x)O_4$ (x = 0.1 and 0.2) ceramics give contributions to the ε_r and phonon absorptions determine the intrinsic dielectric loss in the microwave region. Combined with the crystal structure, thermal expansion, and microwave dielectric properties above, this novel mechanism to tune TCF is feasible in other LnNbO$_4$ (Ln = lanthanide) microwave dielectric ceramics, proved by far-infrared reflectivity analysis where the ionic polarization mainly dominates the microwave ε_r and dielectric loss. The comparisons of microwave dielectric properties of K20 materials discussed here are listed in Table 1 for comparison with other K20s. Taking advantage of the permittivity "valley" of LnNbO$_4$ (Ln = lanthanide) materials at ferroelastic phase transition, near-zero TCF values could be achieved by rational design.

4. Conclusions

The substitution V over Nb in the NdNbO$_4$ ceramic lowered the ferroelastic phase transition (T_{F-S}) from 720 °C of NdNbO$_4$ to 400 °C of $Nd(Nb_{0.8}V_{0.2})O_4$, resulting in not only a minimum occurrence in permittivity at T_{F-S} in $Nd(Nb_{0.9}V_{0.1})O_4$ and $Nd(Nb_{0.8}V_{0.2})O_4$ ceramics at 600 °C and 400 °C, respectively, but also an abrupt

change in thermal expansion coefficient. The negative temperature coefficient of permittivity and positive thermal expansion coefficient of the $Nd(Nb_{0.8}V_{0.2})O_4$ ceramic leads to a near-zero temperature coefficient of resonant frequency. Excellent microwave dielectric properties performance could be achieved in the $Nd(Nb_{0.8}V_{0.2})O_4$ ceramic with the permittivity ~ 18.6, the Qf ~ 70,100 GHz and the TCF ~ +7.8 ppm/°C. Eventually, a novel method of tuning temperature stability in microwave dielectric ceramics with high Qf value in the $Nd(Nb_{1-x}V_x)O_4$ ($0 \leq x \leq 0.2$) ceramics is demonstrated through adjusting T_{F-S} with an associated modification of α_L and τ_ε. Further study on modifications of the wide temperature stability will benefit various applications of microwave dielectric devices.

Declaration of Competing Interest

The authors declare no competing interests.

Acknowledgements

References

(1) Sebastian, M. T.; Jantunen, H. Low Loss Dielectric Materials for LTCC Applications: A Review. *Int. Mater. Rev.* **2008**, *53*, 57–90.

(2) Reaney, I. M.; Iddles, D. M. Microwave Dielectric Ceramics for Resonators and Filters in Mobile Phone Networks. *J. Am. Ceram. Soc.* **2006**, *89,* 2063−2072.

(3) Wu, F. F.; Zhou, D.; Du, C.; Jin, B. B.; Li, C.; Qi, Z. M.; Sun, S. K.; Zhou, T.; Li, Q.; Zhang, X. Design of a Sub-6 GHz Dielectric Resonator Antenna with Novel Temperature Stabilized $(Sm_{1-x}Bi_x)NbO_4$ (x=0-0.15) Microwave Dielectric Ceramics. *ACS Appl. Mater. Interfaces* **2022**, *14[5]*, 7030–7038.

(4) Du, C.; Fu, M. S.; Zhou, D.; Guo, H. H.; Chen, H. T.; Zhang J.; Wang, J. P.; Wang, S. F.; Liu, H. W.; Liu, W. F.; Li, L.; Xu, Z. Dielectric Resonator Antenna with $Y_3Al_5O_{12}$ Transparent Dielectric Ceramics for 5G Millimeter-Wave Applications. *J. Am. Ceram. Soc.* **2021**, *104[9]*, 4659-4668.

(5) Qin J. C.; Liu Z. F.; Ma, M. S.; Liu, F.; Qi, Z. M.; Li, Y. X. Structure and Microwave Dielectric Properties of Gillespite-Type $ACuSi_4O_{10}$ (A = Ca, Sr, Ba) Ceramics and Quantitative Prediction of the Q×f Value via Machine Learning. *ACS Appl. Mater. Interfaces* **2021**, *13[15]*, 17817-17826.

(6) Elijah, O.; Leow, C. Y.; Rahman, T. A.; Nunoo, S.; Iliya, S. Z. Comprehensive Survey of Pilot Contamination in Massive MIMO 5G System. *IEEE Commun. Surv. Tutorials* **2016**, *18*, 905−923.

(7) Xiao, K.; Gong, L.; Kadoch, M. Opportunistic Multicast NOMA with Security Concerns in a 5G Massive MIMO System. *IEEE Commun. Mag.* **2018**, *56*, 91−95.

(8) Khan, I.; Zafar, M.; Jan, M.; Lloret, J.; Basheri, M.; Singh, D. Spectral and Energy Efficient Low-Overhead Uplink and Downlink Channel Estimation for 5G Massive

MIMO Systems. *Entropy* **2018**, *20*, 92.

(9) Liu, F.; Guo, J.; Zhao, L.; Shen, X.; Yin, Y. A Meta-Surface Decoupling Method for Two Linear Polarized Antenna Array in Sub-6 GHz Base Station Applications. *IEEE Access* **2019**, *7*, 2759−2768.

(10) Li, H.; Tang, B.; Li, X.; Qing, Z.; Li, Y.; Yang, H.; Wang, Q.; Zhang, S. The Structure and Properties of $0.95MgTiO_3–0.05CaTiO_3$ Ceramics Doped with Co_2O_3. *J. Mater. Sci.* **2014**, *49*, 5850–5855.

(11) H. Jantunen, R. Rautioaho, A. UusimaÈki, S. LeppaÈvuori, Compositions of $MgTiO_3-CaTiO_3$ Ceramic with Two Borosilicate Glasses for LTCC Technology. *J. Eur. Ceram. Soc.* **2000**, *20*, 2331-2336.

(12) Huang, C. L.; Chen, J. Y.; Li, B. J. A New Dielectric Material System Using $(1 − x)(Mg_{0.95}Co_{0.05})_2TiO_4–xCa_{0.8}Sm_{0.4/3}TiO_3$ at Microwave Frequencies. *Mater. Chem. Phys.* **2010**, *120*, 217–220.

(13) Huang, C. L.; Chen, J. Y.; Huang G. S. A New Low-loss Dielectric using $CaTiO_3$-Modified $(Mg_{0.95}Mn_{0.05})TiO_3$ Ceramics for Microwave Applications. *J. Alloys Comp.* **2010**, 499, 48–52.

(14) Huang, C. L.; Chen, J. Y.; Li B. J. A New Dielectric Material System using $(1-x)(Mg_{0.95}Co_{0.05})_2TiO_4–xCa_{0.8}Sm_{0.4/3}TiO_3$ at Microwave Frequencies. *Mater. Chem. Phys.* **2010**, 120, 217–220.

(15) Huang, C. L.; Liu S.S. Dielectric Characteristics of the $(1-x)Mg_2TiO_4–xSrTiO_3$ Ceramic System at Microwave Frequencies. *J. Alloys Comp.* **2009**, 471, L9–L12.

(16) Huang, C. L.; Liu S.S. High-Q Microwave Dielectric in the $(1−x)MgTiO_3–xCa_{0.6}La_{0.8/3}TiO_3$ Ceramic System with A Near-zero Temperature

Coefficient of the Resonant Frequency. *Mater. Lett.* **2008**, 62, 3205–3208.

(17) Fan, X. C.; Chen, X. M. Effects of Ca/Ti Co-Substitution upon Microwave Dielectric Characteristics of CaSmAlO$_4$ Ceramics. *J. Am. Ceram. Soc.* **2009**, *92*, 433–438.

(18) Ren, G. R.; Zhu, J. Y.; Li, L.; Liu, B.; Chen, X. M. SrLa(R$_{0.5}$Ti$_{0.5}$)O$_4$ (R=Mg, Zn) Microwave Dielectric Ceramics with Complex K$_2$NiF$_4$-Type Layered Perovskite Structure. *J. Am. Ceram. Soc.* **2017**, *100[6]*, 2582-2589.

(19) Mao, M. M.; Chen, X. M.; Liu, X. Q. Structure and Microwave Dielectric Properties of Solid Solution in SrLaAlO$_4$-Sr$_2$TiO$_4$ System. *J. Am. Ceram. Soc.* **2011**, *94[11]*, 3948-3952.

(20) Liu, B.; Yi, L.; Li L.; Chen, X. M. Densification and Microwave Dielectric Properties of Ca$_{1.15}$Sm$_{0.85}$Al$_{0.85}$Ti$_{0.15}$O$_4$ Ceramics with B$_2$O$_3$ Addition. *J. Alloys Comp.* **2015**, 653, 351-357.

(21) Mao, M. M.; Fan, X. C.; Chen, X. M. Effect of A-Site Ionic Radius on the Structure and Microwave Dielectric Characteristics of Sr$_{1+x}$Sm$_{1-x}$Al$_{1-x}$Ti$_x$O$_4$ Ceramics, *Int. J. Appl. Ceram. Technol.* **2010**, 7, E156-E162.

(22) Xiao, Y.; Chen, X. M.; Liu, X. Q. Microstructures and Microwave Dielectric Characteristics of CaRAlO$_4$ (R = Nd, Sm, Y) Ceramics with Tetragonal K$_2$NiF$_4$ Structure. *J. Am. Ceram. Soc.* **2004**, 87, 2143-2146.

(23) Pang, L. X.; Zhou, D. Microwave Dielectric Properties of Low-Firing Li$_2$MO$_3$ (M = Ti, Zr, Sn) Ceramics with B$_2$O$_3$-CuO Addition. *J. Am. Ceram. Soc.* **2010**, *93[11]*, 3614-3617.

(24) Bian, J. J.; Dong, Y. F. New High Q Microwave Dielectric Ceramics with Rock Salt Structures: $(1-x)$Li$_2$TiO$_3$+xMgO System ($0 \leq x \leq 0.5$). *J. Eur. Ceram. Soc.* **2010**, *30*, 325−330.

(25) Guo, H. H.; Fu, M. S.; Zhou, D.; Du, C.; Wang, P. J.; Pang, L. X.; Liu, W. F.; Sombra, A. S. B.; Su, J. Z. Design of High Efficiency and Gain Antenna Using Novel Low Loss, Temperature Stable $Li_2Ti_{1-x}(Cu_{1/3}Nb_{2/3})_xO_3$ Microwave Dielectric Ceramics. *ACS Appl. Mater. Interfaces*, **2021**, *13[1]*, 912–923.

(26) Guo, H. H.; Zhou, D.; Du, C.; Wang, P. J.; Liu, W. F.; Pang, L. X.; Wang, Q. P.; Su, J. Z.; Singh, C.; Trukhanov, S. Temperature Stable $Li_2Ti_{0.75}(Mg_{1/3}Nb_{2/3})_{0.25}O_3$ Based Microwave Dielectric Ceramics with Low Sintering Temperature and Ultra-Low Dielectric Loss for Dielectric Resonator Antenna Applications. *J. Mater. Chem. C* **2020**, *8*, 4690-4700.

(27) Kim, D. W.; Kwon, D. K.; Yoon, S. H.; Hong, K. S. Microwave Dielectric Properties of Rare-Earth Ortho-Niobates with Ferroelasticity. *J. Am. Ceram. Soc.* **2006**, *89*, 3861−3864.

(28) McCarthy, G. J. X-Ray Studies of $RENbO_4$ Compounds. *Acta Cryst.* **1971**, *B27*, 2285–2286.

(29) Zhang, P.; Song, Z.; Wang, Y.; Li, L. Effect of Ion Substitution for Nd^{3+} Based on Structural Characteristic on the Microwave Dielectric Properties of $NdNbO_4$ Ceramic System. *J. Am. Ceram. Soc.* **2014**, *97*, 976−981.

(30) Pang, L. X.; Zhou, D. Modification of $NdNbO_4$ Microwave Dielectric Ceramic by Bi Substitutions. *J. Am. Ceram. Soc.* **2019**, *102*, 2278−2282.

(31) Ramarao, S. D.; Murthy, V. R. K. Structural Phase Transformation and Microwave Dielectric Studies of $SmNb_{1-x}(Si_{1/2}Mo_{1/2})_xO_4$ Compounds with Fergusonite Structure. *Phys. Chem. Chem. Phys.* **2015**, *17*, 12623−12633.

(32) Lim, H.; Oh, Y. J. Low-Temperature Sintered $Bi_{1-x}Sm_xNbO_4$ Microwave Dielectrics. *J. Eur. Ceram. Soc.* **2020**, *40*, 1191−1197.

(33) Zhou, D.; Guo, H. H.; Fu, M. S.; Yao, X. G.; Lin, H. X.; Liu, W. F.; Pang, L. X.;

Singh, C.; Trukhanov, S.; Trukhanov, A.; Reaney, I. M. Anomalous Dielectric Behaviour During the Monoclinic to Tetragonal Phase Transition in La($Nb_{0.9}V_{0.1}$)O_4. *Inorganic Chemistry Frontiers*, **2021**, *8*, 156−163.

(34) Krupka, J.; Derzakowski, K.; Riddle, B.; Baker-Jarvis, J. A Dielectric Resonator for Measurements of Complex Permittivity of Low Loss Dielectric Materials as A Function of Temperature. *Meas. Sci. Technol.* **1998**, 9, 1751−1756.

(35) Shannon, R. D. Revised Effective Ionic Radii and Systematic Studies of Interatomic Distances in Halides and Chalcogenides. *Acta Cryst.* **1976**, *A32*, 751-767.

(36) Roth, R.S.; Waring, J. L. Phase Equilibrium Relations in the Binary System Bismuth Sesquioxide-Niobium Pentoxide. *J. Res. National Bureau Standards Sec. A-Phys. Chem.* **1962**, *66[6]*, 451-463.

(37) Mani, R.; Bhuvanesh, N. S. P.; Ramanujachary, K. V.; Green, W.; Lofland, S. E.; Gopalakrishnan, J. A Novel One-Pot Metathesis Route for The Synthesis of Double Perovskites, $Ba_3MM'_2O_9$ (M = Mg, Ni, Zn; M'= Nb, Ta) with 1 : 2 Ordering of M and M' Atoms. *J. Mater. Chem.* **2007**, *17*, 1589-1592.

(38) Zhou, D.; Pang, L. X.; Wang, D. W.; Reaney, I. M. $BiVO_4$ Based High k Microwave Dielectric Materials: A Review. *J. Mater. Chem. C* **2018**, *6*, 9290-9313.

(39) Yamauchi, H.; Tsunekawa, S.; Tomiyoshi, S.; Fukuda, T.; Kamiyama, T.; Asano, H. Anomalous Paramagnetic Property of $NdNbO_4$ Single Crystals. *J. Phys. Soc. Japan*, **1990**, *59[7]*, 2602-2603.

(40) Tsunekawa, S.; Kamiyama, T.; Sasaki, K.; Asano, H.; Fukuda, T. Precise Structure Analysis by Neutron Diffraction for $RNbO_4$ and Distortion of NbO_4 Tetrahedra. *Acta Crystallographica A* **1993**, *49*, 595-600.

(41) Shannon, R. D. Dielectric Polarizabilities of Ions in Oxides and Fluorides. *J. Appl. Phys.* **1993**, *73*, 348−366.

Table 1 Microwave dielectric properties of K20 materials

System	S. T. (°C)	ε_r	Qf (GHz)		TCF (ppm/°C)	Ref.
$MgTiO_3$ / Mg_2TiO_4 - $(Ca,Ln)TiO_3$, Ln = lanthanide	1250 ~1350	19~23	60,000 10,000	~	−5 ~ +5	10-16
$(Ca,Sr)LnAlO_4$, Ln= lanthanide	1400 ~1550	18~20	30,000 50,000	~	−10 ~ +10	22
$(Ca,Sr)Ln(Al,Ti)O_4$, Ln= lanthanide	1450 ~1550	19~22	80,000 10,000	~	−5 ~ +5	17-21
$Li_2(Ti, (M^{2+}_{1/3}M^{5+}_{2/3}))O_3$, M^{2+}=Zn, Mg, Cu; M^{5+}=Nb, Ta	1000 ~1200	18~20	60,000 10,000	~	−5 ~ +5	23-26
$LnNbO_4$, Ln= lanthanide	1250 ~1500	18~20	30,000 60,000	~	−40 ~ +10	27
$Ln(Nb,V)O_4$, Ln= lanthanide	1250 ~1400	17~20	40,000 80,000	~	−5 ~ +5	28-33

Table 2 Refined atomic fractional coordinates from XRD data for $Nd(Nb_{0.9}V_{0.1})O_4$ sample at room temperature and the lattice parameters are a = 5.4367(5) Å, b = 11.3356(6) Å, c = 5.1590 (7) Å, β = 93.699(3)°. The space group is I12/c1 (No. 15).

Atom	Site	Occ.	x	y	z	B (Å^2)
Nd	4e	0.5	0.2500	0.1203(1)	0.0000	0.65(6)
Nb	4e	0.45	0.2500	0.6433(1)	0.0000	0.39(3)
V	4e	0.05	0.2500	0.6433(1)	0.0000	0.39(3)
O1	8f	1.00	0.0068(7)	0.7097(2)	0.1913(9)	1.10(5)
O2	8f	1.00	0.9241(7)	0.4482(3)	0.2414(3)	2.17(1)

Table 3 Refined atomic fractional coordinates from XRD data for $Nd(Nb_{0.8}V_{0.2})O_4$ sample at room temperature and the lattice parameters are a = 5.3982(9) Å, b = 11.3828(7) Å, c = 5.1751(9) Å, β = 92.865(1)°. The space group is I12/c1 (No. 15).

Atom	Site	Occ.	x	y	z	B (Å^2)
Nd	4e	0.5	0.2500	0.1215(3)	0.0000	0.26(2)
Nb	4e	0.4	0.2500	0.6398(5)	0.0000	0.38(7)
V	4e	0.1	0.2500	0.6398(5)	0.0000	0.38(7)
O1	8f	1.00	0.0146(5)	0.7121(8)	0.1849(4)	2.31(1)
O2	8f	1.00	0.9218(1)	0.4549(8)	0.2377(2)	1.41(3)

Figures Captions

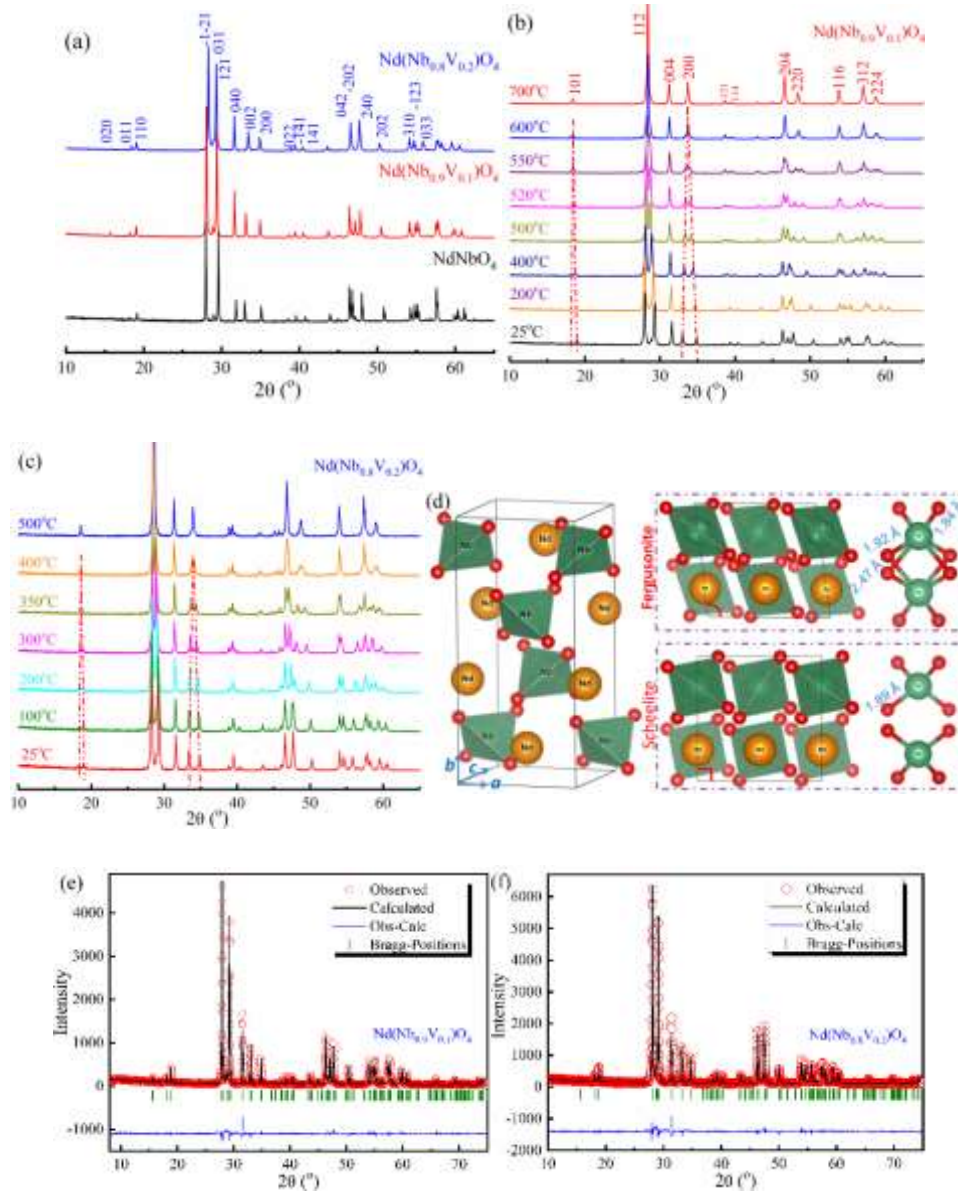**Fig. 1.** (a) Room temperature PXRD patterns of the $Nd(Nb_{1-x}V_x)O_4$ ($0 \leq x \leq 0.2$) ceramics, (b) *in-situ* high temperature PXRD patterns of the $Nd(Nb_{0.9}V_{0.1})O_4$, (c) $Nd(Nb_{0.8}V_{0.2})O_4$, (d) schematics of the crystal structures of fergusonite and scheelite crystal structures and associated refinements of $Nd(Nb_{1-x}V_x)O_4$ for $0 \leq x \leq 0.2$, experimental (circles) and calculated (line) XRD profiles for the $Nd(Nb_{0.9}V_{0.1})O_4$ (e) with R_p = 8.39 %, R_{wp} = 11.4 %, R_{exp} = 9.31 %, (a) and $Nd(Nb_{0.8}V_{0.2})O_4$ (f) sample at room temperature with R_p = 6.31 %, R_{wp} = 8.44 %, R_{exp} = 6.59 %, (The short vertical lines below the patterns mark the positions of Bragg reflections. The bottom continuous line is the difference between the observed and the calculated intensity.)

Fig. 2. The unit cell parameters (a) and the thermal expansion data (b) of $Nd(Nb_{0.9}V_{0.1})O_4$ and $Nd(Nb_{0.8}V_{0.2})O_4$ as a function to temperature.

Fig. 3. HRTEM images of the $Nd(Nb_{0.9}V_{0.1})O_4$ ceramic (a) and (c) in left, and the $Nd(Nb_{0.8}V_{0.2})O_4$ ceramic (b) and (d) in right.

Fig. 4. SEM images of the thermal etched surfaces of the $Nd(Nb_{1-x}V_x)O_4$ ($0 \leq x \leq 0.2$) ceramics sintered at optimal temperatures (a) x = 0 sintered at 1300 ℃, (b) x = 0.1 sintered at 1280 ℃ and (c) x = 0.2 sintered at 1280 ℃.

Fig. 5. Relative permittivity (a) and dielectric loss (b) of the $Nd(Nb_{1-x}V_x)O_4$ (x = 0.1 and 0.2) (not clear in the figure) ceramics as a function of temperature at different frequencies (100 kHz, 250 kHz, 1 MHz and 7.2 GHz).

Fig. 6. Microwave permittivity, Qf values (a), TCF values and phase transition temperatures (b) of the $Nd(Nb_{1-x}V_x)O_4$ ($0 \leq x \leq 0.2$) ceramics as a function of x.

Fig. 7. Measured and calculated infrared reflectivity spectra and complex permittivity of the Nd(Nb$_{1-x}$V$_x$)O$_4$ (x=0.1 and 0.2) ceramics (solid line for fitting values and circle for measured values)

Fig. 1. (a) Room temperature PXRD patterns of the Nd(Nb$_{1-x}$V$_x$)O$_4$ ($0 \leq x \leq 0.2$) ceramics, (b) *in-situ* high temperature PXRD patterns of the Nd(Nb$_{0.9}$V$_{0.1}$)O$_4$, (c) Nd(Nb$_{0.8}$V$_{0.2}$)O$_4$, (d) schematics of the crystal structures of fergusonite and scheelite crystal structures and associated refinements of Nd(Nb$_{1-x}$V$_x$)O$_4$ for $0 \leq x \leq 0.2$, experimental (circles) and calculated (line) XRD profiles for the Nd(Nb$_{0.9}$V$_{0.1}$)O$_4$ (e) with R$_p$ = 8.39 %, R$_{wp}$ = 11.4 %, R$_{exp}$ = 9.31 %, (a) and Nd(Nb$_{0.8}$V$_{0.2}$)O$_4$ (f) sample at

room temperature with R_p = 6.31 %, R_{wp} = 8.44 %, R_{exp} = 6.59 %, (The short vertical lines below the patterns mark the positions of Bragg reflections. The bottom continuous line is the difference between the observed and the calculated intensity.)
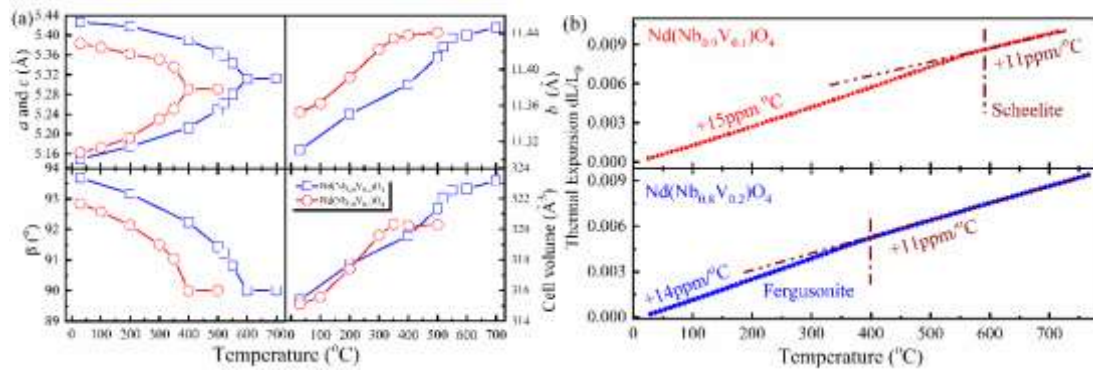

Fig. 2. The unit cell parameters (a) and the thermal expansion data (b) of Nd(Nb$_{0.9}$V$_{0.1}$)O$_4$ and Nd(Nb$_{0.8}$V$_{0.2}$)O$_4$ as a function to temperature.

Fig. 3. HRTEM images of the $Nd(Nb_{0.9}V_{0.1})O_4$ ceramic (a) and (c) in left, and the
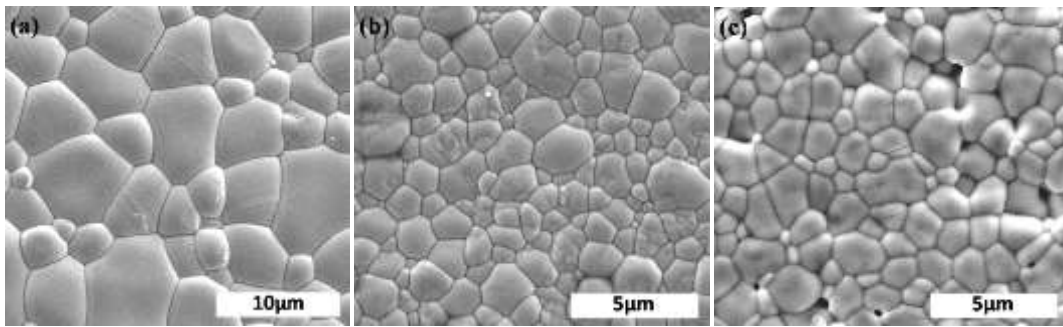
$Nd(Nb_{0.8}V_{0.2})O_4$ ceramic (b) and (d) in right.

Fig. 4. SEM images of the thermal etched surfaces of the $Nd(Nb_{1-x}V_x)O_4$ $(0 \leq x \leq 0.2)$ ceramics sintered at optimal temperatures (a) $x = 0$ sintered at 1300 °C, (b) $x = 0.1$ sintered at 1280 °C and (c) $x = 0.2$ sintered at 1280 °C.
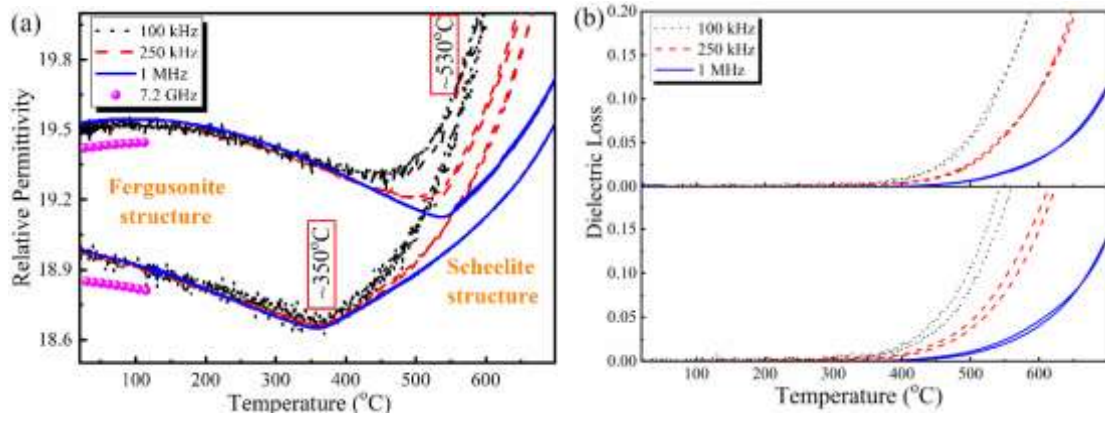
Fig. 5. Relative permittivity (a) and dielectric loss (b) of the Nd(Nb$_{1-x}$V$_x$)O$_4$ ($x = 0.1$ and 0.2) (not clear in the figure) ceramics as a function of temperature at different frequencies (100 kHz, 250 kHz, 1 MHz and 7.2 GHz).
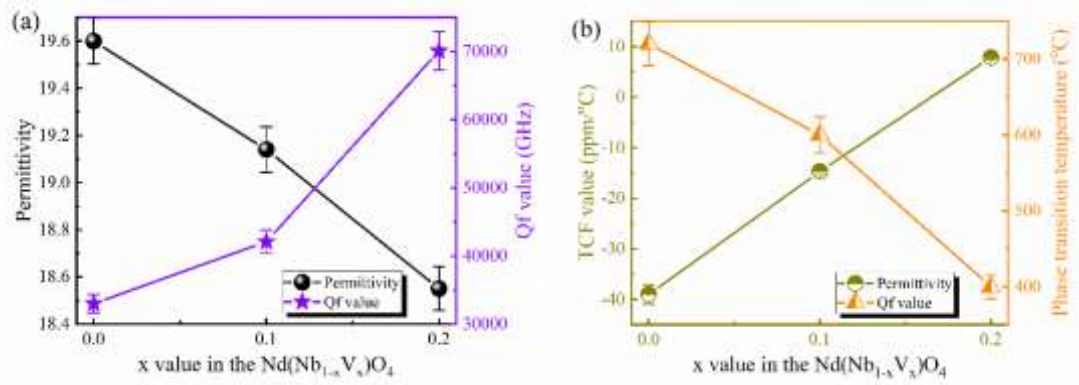
Fig. 6. Microwave permittivity, Qf values (a), TCF values and phase transition temperature (b) of the Nd(Nb$_{1-x}$V$_x$)O$_4$ ($0 \leq x \leq 0.2$) ceramics as a function of x.
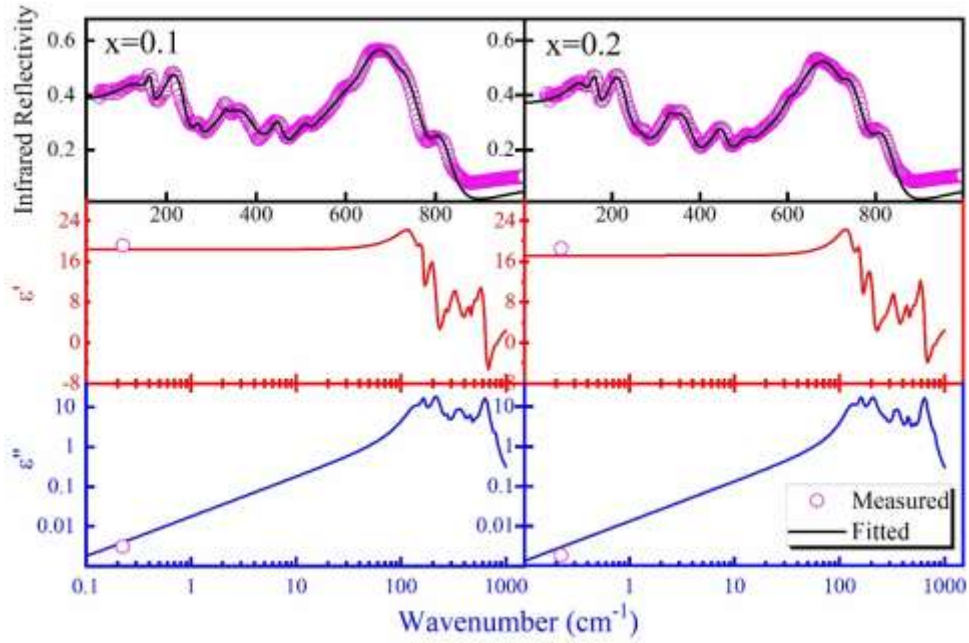
Fig. 7. Measured and calculated infrared reflectivity spectra and complex permittivity of the Nd(Nb$_{1-x}$V$_x$)O$_4$ (x=0.1 and 0.2) ceramics (solid line for fitting values and circle for measured values)

Table Of Contents (TOC) graphic

Nd(Nb$_{0.8}$V$_{0.2}$)O$_4$, ε$_r$=18.6, Qf = 70,100 GHz, TCF = +7.8 ppm/°C